Pharm Res (2012) 29:2317–2328
DOI 10.1007/s11095-012-0758-9

RESEARCH PAPER

Selective Targeting of c-Abl via a Cryptic Mitochondrial Targeting Signal Activated by Cellular Redox Status in Leukemic and Breast Cancer Cells

Jonathan E. Constance • Samuel D. Despres • Akemi Nishida • Carol S. Lim

Received: 8 February 2012 / Accepted: 11 April 2012 / Published online: 2 May 2012

ABSTRACT

Purpose The tyrosine kinase c-Abl localizes to the mitochondria under cell stress conditions and promotes apoptosis. However, c-Abl has not been directly targeted to the mitochondria. Fusing c-Abl to a mitochondrial translocation signal (MTS) that is activated by reactive oxygen species (ROS) will selectively target the mitochondria of cancer cells exhibiting an elevated ROS phenotype. Mitochondrially targeted c-Abl will thereby induce malignant cell death.

Methods Confocal microscopy was used to determine mitochondrial colocalization of ectopically expressed c-Abl-EGFP/cMTS fusion across three cell lines (K562, Cos-7, and 1471.1) with varying levels of basal (and pharmacologically modulated) ROS. ROS were quantified by indicator dye assay. The functional consequences of mitochondrial c-Abl were assessed by DNA accessibility to 7-AAD using flow cytometry.

Results The cMTS and cMTS/c-Abl fusions colocalized to the mitochondria in leukemic (K562) and breast (1471.1) cancer phenotypes (but not Cos-7 fibroblasts) in a ROS and PKC dependent manner.

Conclusions We confirm and extend oxidative stress activated translocation of the cMTS by demonstrating that the cMTS and Abl/cMTS fusion selectively target the mitochondria of K562 leukemia and mammary adenocarcinoma 1471.1 cells. c-Abl induced K562 leukemia cell death when targeted to the matrix but not the outer membrane of the mitochondria.

KEY WORDS c-Abl · cryptic MTS · mitochondria · reactive oxygen species · translocation

ABBREVIATIONS

c-Abl	Abelson proto-oncoprotein
CML	chronic myelogenous leukemia
cMTS	cryptic mitochondrial translocation sequence
EGFP	enhanced green fluorescent protein
JACoP	Just Another Colocalization Plugin
mGSTA4-4	murine glutathione-S-transferase A4-4
MOM	mitochondrial outer membrane
PCC	Pearson's correlation coefficient
PKA	protein kinase A
PKC	protein kinase C
PMA	phorbol myristate acetate
ROI	region of interest
ROS	reactive oxygen species
S	serine
T	threonine
TKI	tyrosine kinase inhibitor
Y	tyrosine

INTRODUCTION

A hyper-oxidative environment is a pathophysiologic hallmark of many disease states, including cancer (1). Cell fate often rests on proteins (e.g., antioxidant enzymes or pro-apoptotic factors) that are responsive to oxidative stress and translocate to the mitochondria (2). However, oncoprotein

C. S. Lim (✉)
Department of Pharmaceutics and Pharmaceutical Chemistry
College of Pharmacy, University of Utah
421 Wakara Way, Rm. 318
Salt Lake City, Utah 84108, USA
e-mail: Carol.Lim@pharm.utah.edu

J. E. Constance
Department of Pharmacology and Toxicology
College of Pharmacy, University of Utah
Salt Lake City, Utah 84108, USA
e-mail: Jonathan.Constance@utah.edu

A. Nishida
College of Pharmacy, University of Utah
Salt Lake City, Utah 84108, USA
e-mail: Akemi.Nishida@pharm.utah.edu

S. D. Despres
University of Utah
Salt Lake City, Utah 84108, USA
e-mail: smdsprs@comcast.net

signaling can disrupt, directly or indirectly, pro-apoptotic signal transduction at the level of the mitochondria (3). For instance, the ubiquitously expressed non-receptor tyrosine kinase c-Abl has been termed a "mitochondrial wracking factor" (4) since active c-Abl translocation to the mitochondria induces cell death (5). In the context of chronic myelogenous leukemia (CML) though, the pro-death functions of c-Abl are prevented by the aberrantly active tyrosine kinase fusion oncoprotein Bcr-Abl (6).

The functional specificity c-Abl is dictated by subcellular location (7). The majority (70 %) of c-Abl resides in the nucleus with about 20 % in the ER and 5–8 % in the cytoplasm with the remainder (~4 %) found in the mitochondria (8). c-Abl can promote mitogenesis when located in cytoplasm, cell cycle arrest when activated in the nucleus, and upon translocation to the mitochondria can induce the loss of mitochondrial membrane potential (ψ_{MIT}), depletion of ATP, and apoptotic/necrotic cell death (8,9). Additionally, c-Abl was the first tyrosine kinase found to associate with the mitochondria (10) and is considered to be the key apoptotic tyrosine kinase (11). At present the submitochondrial location and substrates for c-Abl are unidentified (12). To our knowledge the consequences of c-Abl to mitochondrial targeting has only been examined in the context of a cellular insult (e.g., H_2O_2, genotoxic agents, and endoplasmic reticulum toxins), and direct targeting of c-Abl to the mitochondria through fusion to a mitochondrial targeting signal (MTS) has not been studied.

Protein localization to different subcellular compartments is often directed by signal sequences encoded in the protein itself. Normally, death-directed c-Abl requires association with a chaperone protein (i.e., PKCδ) to reach the mitochondria as it does not contain an MTS of its own (9). MTSs are usually found at the N- or C-terminus of proteins (13) but fusions to the N-terminus of c-Abl (e.g., Bcr-Abl) disrupt its normal conformation (14). Therefore, in order to permit c-Abl to adopt its native conformation a C-terminal fusion is required. One such C-terminal MTS, that conditionally targets the mitochondria, is derived from murine glutathione-S-transferase A4-4 (GSTA4-4; C-terminal residues 172–222) (15).

The GSTA4-4 MTS is considered a 'cryptic' MTS (cMTS) and was previously shown to translocate from the cytosol to the mitochondria in Cos cells under pharmacological stimulation of oxidative stress or protein kinase activators (15,16). The mitochondrial translocation of the cMTS is dependent upon activation, via phosphorylation. Key cMTS residues, S189 and T193, are phosphorylated by the protein kinase A (PKA) and/or protein kinase C (PKC) family of ser/thr kinases, respectively. A dihydrofolate reductase/cMTS fusion was previously shown to localize in the mitochondria of Cos cells upon protein kinase activator stimulation (15). Therefore, this study aims to determine if the cMTS could provide a means to selectively target pro-apoptotic c-Abl to the mitochondria based on the inherent level of intracellular reactive oxygen species (ROS) as a discriminating factor across cell types.

Elevated intracellular ROS can lead to the activation of transcription factors (e.g., HIF-1 and NF-κB) leading to a host of protein expression profiles that contribute to malignancy such as proliferation, survival, and metastasis. This situation leads to a seeming 'ROS paradox' where many antineoplastic agents, like imatinib, exert their cytotoxic effects through the generation of ROS. The underlying mechanisms for (the essential) ROS mediated killing by chemotherapeutics and radiation therapy is not well understood (17). However, an increase in magnitude of the already elevated ROS in cancer cells is likely to exceed the antioxidant capacity of the cancer and cause cell death (18).

A small selection of cell lines exhibiting different levels of basal ROS were used to test the selective mitochondrial accumulation of cMTS-containing constructs. First, human leukemia K562 cells are characterized by elevated ROS and serve as a representative of a cell type in a pathologic pro-oxidative state. K562 cells have high basal levels of ROS due to Bcr-Abl's stimulation of the PI3K/mTOR pathway leading to overactivation of the mitochondrial electron transport chain (19). The oncogenic Bcr-Abl (present in K562) engages signaling pathways that result in the production of ROS, causing CML cells to have a high cellular oxidative stress background (20). Therefore, ROS levels are chronically elevated due to the presence of Bcr-Abl. Even when Bcr-Abl activity is blocked by tyrosine kinase inhibitor therapy, ROS production is induced via another (apoptotic) route (21). Secondly, both chronic ROS and PKC over-activation have been associated with breast cancer (22,23); therefore, the murine mammary adenocarcinoma 1471.1 cell line was included. Finally, the transformed monkey kidney fibroblast Cos-7 cell line was used as a negative control for background ROS. Within the context of the elevated ROS K562 cell line, antioxidants (α-tocopherol and N-acetylcysteine) and an antineoplastic (imatinib) were used to modulate the level of ROS, and the consequent effects on mitochondrial localization of constructs was determined.

MATERIALS AND METHODS

Materials

RPMI-1640 medium, MitoTracker Red CM-H_2XRos (MitoTracker CMXros), 7-aminoactinomycin D (7-AAD; DNA intercalating dye permeable to dying or dead cells), 5-(and-6)-carboxy-2′,7′-dichlorofluoroescein (carboxy-H_2DCFDA; general oxidative stress indicator), Lipofectamine LTX with Plus reagent, and phosphate-

buffered saline (PBS) were purchased from Invitrogen (Carlsbad, CA). Penicillin-streptomycin-L-glutamine (P-S-G; 100U/mL), DMEM media and trypsin were purchased from Gibco BRL (Grand Island, NY). Fetal bovine serum (FBS) and gentamycin were purchased from Hyclone Laboratories (Logan, UT). The (+)-α-tocopherol type VI (α-Toc), N-acetyl-L-cysteine (NAC), and poly-L-lysine (0.01 % solution) were purchased from Sigma-Aldrich (St. Louis, MO). Imatinib (CT-IM001) was purchased from ChemieTek (Indianapolis, IN). QuikChange II XL Site-Directed Mutagenesis Kit was purchased from Agilent Technologies (Santa Clara, CA). Cell Line Nucleofector Kit V was purchased from Lonza Group (Basel, Switzerland).

Cell Lines and Culture Conditions

K562 cells (non-adherent human chronic myelogenous leukemia cell line, gift from Dr. K. Elenitoba-Johnson, University of Michigan), and Cos-7 (monkey kidney fibroblast adherent cell line; ATCC) were cultured in RPMI 1640 supplemented with 10 % FBS, 1 % P-S-G (GIBCO BRL, Grand Island, NY), and 0.1 % gentamycin. Murine mammary adenocarcinoma 1471.1 cells, (gift from Gordon Hager, PhD, NCI, NIH) were grown as monolayers in with DMEM supplemented with 10 % FBS, 1 % P-S-G and 0.1 % gentamycin. K562 cells were passaged at a density of 0.5×10^5/mL every other day, and discontinued at the tenth passage. Cos-7 and 1471.1 cells were passaged at 80 % confluency and split 1:10 in fresh media and discontinued after passage 15. All cells were maintained in a 5 % CO_2 incubator at 37°C.

Expression of Constructs in K562 Leukemia, Cos-7 Fibroblast, and 1471.1 Breast Cancer Cells

Constructs were transiently transfected into K562 cells using the Amaxa Nucleofector II, as described previously (24). Briefly, 2×10^6 K562 cells, between passages 5–10, were pelleted prior to a 48 h initial seed density of 0.5×10^5 cells/mL. Cells were resuspended in 100 µL Amaxa Solution V, combined with 2 µg of DNA and transfected in an Amaxa cuvette under program T-013. Transfected cells were immediately transferred to a 25 cm^2 flask with 7 mL of pre-warmed complete RPMI. Transient transfection of 1471.1 and Cos-7 cell were carried out in two-well live-cell chambers (Lab-Tek chamber slide system, Nalge NUNC International, Naperville, IL) or sterile 6-well tissue culture plates (Greiner CellStar, Greiner Bio-one GmbH) using Lipofectamine LTX as per manufacturers' instructions between passages 3 and 15 in antibiotic-free media.

Subcloning and Construction of Plasmids

The murine glutathione S-transferase A4-4 [Swiss-Prot: P24472.3] cMTS (N-terminal residues, 172–222 (15); 51 % sequence homology to human wherein S189 and T193 are conserved) was constructed by annealing four oligonucleotides (**1**: (5′phosphorylated) 5′ -AATTCCGC CCCCGTGCTGAGCGACTTCCCCCTGCTGCAGG CCTTCAAGACCAGAATCAGCAACATCCCCACCA TCAAGAAGTTCCTGCAGCCC-3′, **2**: 5′ -CTGCCG GGCTGCAGGAACTTCTTGATGGTGGGGATGT TGCTGATTCTGGTCTTGAAGGCCTGCAG CAGGGGGAAGTCGCTCAGCACGGGGGCGG-3′, **3**: 5′ -GGCAGCCAGAGAAAGCCCCCCCCCGACGG CCCCTACGTGGAGGTGGTGAGAACCGTGCT GAAGTTCGGCGCCGGCTGCTGCCCCGGCTG CTGCTGA-3′, **4**: (5′ phosphorylated) 5′ -AATTTCAGCA GCAGCCGGGGGCAGCAGCCGGCGCCGAAC TTCAGCACGGTTCTCACCACCTCCACGTAG GGGCCGTCGGGGGGGGGCTTTCTCTGG-3′) simultaneously and then inserting the annealed product into the multiple cloning site (MCS) of EGFP-C1 vector (Promega Biotech, Madison, WI) at the EcoRI (New England Biolabs, Ipswich, MA) site creating pE-cMTS. The pE-cMTS-SY (T186E/R187A/S189Y) and pE-cMTS-TY (P192I/T193Y) were created using site-directed mutagenesis using primers, 5′-GCTGCAGGCCTCAAGGAGGCC ATCTACAACATCCCCACC-3′ and 5′-GACCAGAAT CAGCAACATCATCTACATCAAGAAGTTCCTG CAGCCCGGCAGCCAGAGAA-3′, respectively, with their reverse compliments. Additionally, a tetracysteine motif tag present in the annealed oligonucleotide cMTS insert, was eliminated from being expressed by site-directed mutagenesis to incorporate a stop codon (Primer: 5′-CCGTGCTGA AGTTCTGAGCCGGCTGCTGCC-3′ and reverse complement). Human c-Abl (ABL1 isoform a; NM_005157) was purchased from DF/HCC DNA Resource Core (http://dnaseq.med.harvard.edu/) as plasmid DNA in vector pJP1563 (clone ID HsCD00039065). DNA encoding c-Abl was amplified through PCR using the primers 5′-CGACGACACCGGTCGCCACCATGTTGGAGATC TGCCTG-3′ (includes Kozak sequence) and 5′-CAGTGACATAGTGCAGAGGGGCGCCGGCGGAC CGGTCGACGAC-3′ and subcloned into pEGFP-C1 (Clontech, Mountain View, CA, USA) and pE-cMTS at the blunted (Quick Blunting Kit, New England Biolabs Inc., Ipswich, MA, USA) Age1 restriction enzyme site. The pAbl-E-cMTS KD (kinase dead; isoform 1a K271A mutation (25)) mutant was created using site-directed mutagenesis with the primer 5′-CTGACGGTGGCCGTGGCGACCTTGAAG GAGGAC-3′ and its reverse complement. The MOM targeting sequence derived from Bcl-X_L was constructed by annealing two complementary 5′ phosphorylated oligonucleotides

each containing BamHI sticky ends (XL oligonucleotide 5′-AGAAAGGGCCAGGAGAGATTCAACAGATG GTTCCTGACCGGCATGACCGTGGCCGGCG TGGTGCTGCTGGGCAGCCTGTTCAGCAGAA AGTGA-3′) and inserting into the BamHI restriction enzyme site of pEGFP-C1 and pAbl-E to create pE-MOM and pAbl-E-MOM, respectively. All constructs were verified by sequence analysis.

Mitochondrial Staining

Aliquots of transfected K562 suspension cells (400 μL) were plated into poly-L-lysine coated 4-well live-cell chambers at least four hours in advance of microscopy. Cells were incubated with MitoTracker Red CM-H_2XRos (K562; 100nM, Cos-7 and 1471.1; 325nM) for 45 min at 37°C and protected from light prior to imaging.

Confocal Microscopy

All images of K562, Cos-7, and 1471.1 live cells were acquired on an Olympus IX81 FV1000-XY spectral confocal microscope (Imaging Core Facility, University of Utah) equipped with 405 diode, 488 argon, and 543 HeNe lasers using a 60X PlanApo oil immersion objective (NA 1.45) using Olympus FluoView software. Excitation and emission filters were as follows: EGFP, 488 nm excitation, emission filter 500–530 nm; MitoTracker Red CM-H_2XRos, 543 nm excitation, emission filter 555–655 nm. Images were collected in sequential line mode with exposure and gain of laser kept constant and below detected pixel saturation for each group of cells. No channel crosstalk was observed. Pixel resolution was kept at 1024×1024 (0–2.5-fold digital zoom) with a pixel dwell time of 12.5 μs.

Image Analysis

Images were analyzed as previously (26). Briefly, original images were saved as 16-bit files preserving meta-data. Images were converted to 8-bit, stacked as separate channels, and corrected for background noise using ImageJ plugin 'BG subtraction from background' in default mode (i.e., mean background intensity outside of cells was subtracted) (27). All experiments were completed in at least triplicate. ROIs to be compared for colocalization were constructed using individual cells to control for cell-to-cell intensity variation in colocalization analysis. Image and statistical analysis was performed with JACoP in ImageJ (28). Pearson's correlation coefficient (PCC) was generated using Costes' automatic threshold algorithm to eliminate manual thresholding bias, increase the accuracy in quantifying low level colocalization, and ensure reproducibility (29,30). The PCC is dependent upon both the pixel intensity and overlap of signal and has a range of +1 (complete colocalization) to −1 (anti-correlation) with zero correlating with random distribution between comparators (28). The PCC threshold for defining colocalization (i.e., colocalization due to co-compartmentalization) is 0.6 as per Bolte and Cordelières (28). Channel one (EGFP) and channel two (MitoTracker CMXros) have been false colored, using ImageJ LUT, cyan and magenta, respectively, for increased visual clarity. Additionally, spatial representation of intensity correlation was included between EGFP tagged proteins and the mitochondria (stained with MitoTracker Red CM-H_2XRos) using the Colocalization Colormap ImageJ plugin. 'Colormap' displays positively correlated pixels in hot colors and negatively correlated pixels in cold colors that can be visually interpreted using the color scale bar (31).

Antioxidant Treatment of K562 Cells

Complete RPMI media containing 50 μM (+)-α-tocopherol or N-acetyl-L-cysteine (300 μM or 5 mM, dissolved in RPMI at 80 mM stock concentration, pH adjusted to 7.4) was added to freshly transfected cells.

ROS Detection Assay

ROS production was measured according to the manufacturer's instructions. Briefly, cellular ROS level was measured by incubating cells (10^6) with 25 μM carboxy-H_2DCFDA in the dark for 45 min at 37°C in a 5 % CO_2 incubator in PBS. Immediately following incubation cells were pelleted via centrifugation and resuspended in 400 μL warmed PBS, split into two wells on a black Corning Costar 96-well plate and measured on a SpectraMax M2 fluorescence plate reader (Molecular Devices, Sunnyvale, CA) with excitation at 485 nm and emission collected at 530 nm wavelengths. Either raw arbitrary fluorescence units were reported or expressed as percent control. Positive controls were H_2O_2 (500 μM) treated cell lines (with and without carboxy-H_2DCFDA) and negative controls were cells in PBS without carboxy-H_2DCFDA and also PBS with carboxy-H_2DCFDA.

Cell Death Assay

Flow cytometric assay of cell death was done as previously (32). Briefly, K562, Cos-7, and 1471.1 cells were collected 48 h post-transfection and resuspended in 500 μL ice cold PBS containing 1 μM 7-aminoactinomycin D (7-AAD) for 30 min prior to analysis. Media from adherent Cos-7 and 1471.1 cells was collected prior to trypsinization of cell monolayer and recombined with the enzymatically released cell population for centrifugation and subsequent resuspension. Analysis and gating was performed on a BD

FACSCanto II (Flow Cytometry Core Facility, University of Utah) on BD FACSDiva software (BD Biosciences, Franklin Lakes, NJ). At least three separate experiments in duplicate were performed. Compensation controls were included with each experiment.

Statistics

Data were shown as mean ± S.E.M. Unpaired t-test, one-way ANOVA with Tukey's (or Dunnett's) post-test, two-way ANOVA with Bonferroni post-test, or two-tailed correlation (as indicated in figure legends), were used to evaluate measurements between experimental data with an N of 3 or greater. Statistical significance was set at $P<0.05$ or adjusted lower in instances of multiple comparisons (by convention $P<0.05$ is represented with *, $P<0.01$ with **, $P<0.001$ with ***). GraphPad Prism Graph 4 (GraphPad, La Jolla, CA) software was used for generating statistics.

RESULTS

K562 Leukemia and 1471.1 Mammary Adenocarcinoma Cells Exhibit Elevated ROS Backgrounds and cMTS Mitochondrial Localization Compared to Cos-7

To assess differences in basal ROS levels between K562 leukemia, mammary adenocarcinoma 1471.1, and the Cos-7(negative control for oxidative stress (15,33)) monkey kidney fibroblast cell lines, the conversion of carboxy-H_2DCFDA to DCF was measured (Fig. 1; y-axis in arbitrary fluorescence units). K562 (left column, Fig. 1a) and 1471.1 mammary adenocarcinoma (right column, Fig. 1a) cells demonstrated an elevated background ROS compared to Cos-7 (middle column, Fig. 1a). The basal ROS level of 1471.1 cells fell between the K562 and Cos-7 reference cell lines.

Confocal fluorescence microscopy (Fig. 1b) paired with statistical analysis was used to determine mitochondrial localization of the cryptic MTS derived from GSTA4-4 (cMTS), fused to EGFP, across cell types. Despite the nearly two-fold higher basal ROS level of K562 over the 1471.1 cell line, the E-cMTS was equally colocalized to the mitochondria of both K562 (left column, Fig. 1c) and 1471.1 (right column, Fig. 1c) cells 24 h post-transfection whereas the E-cMTS remained cytosolic in Cos-7 (Fig. 1c, middle column). Figure 1b shows representative images for each cell line transfected with E-cMTS (cyan) and stained with MitoTracker Red (magenta) with white scale bars in the E-cMTS images measuring 5 μm. Image analysis, from at least three separate experiments quantifying the degree of colocalization of the E-cMTS with the mitochondria was used to construct Fig. 1c. The 'degree of colocalization' is

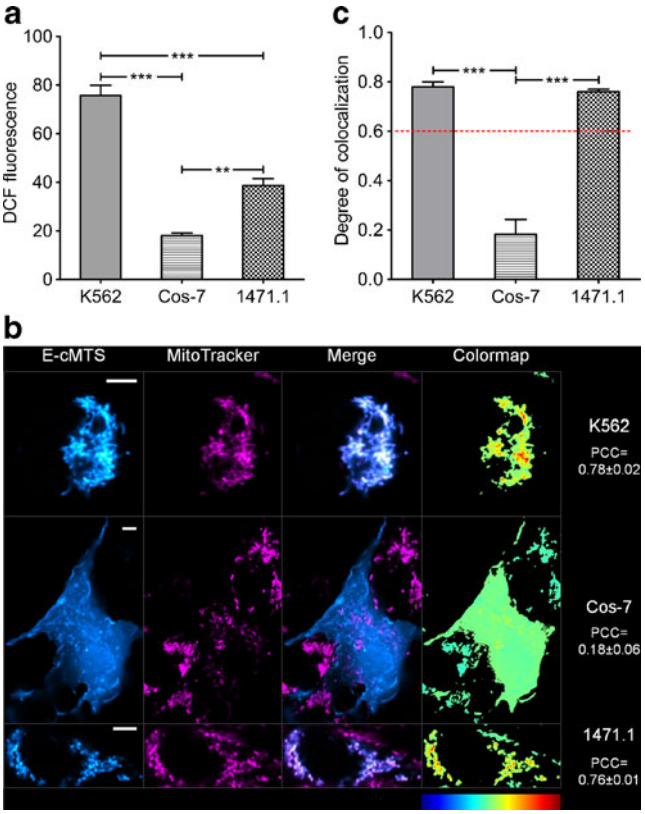

Fig. 1 The cMTS is mitochondrial in K562 and 1471.1 cells but cytosolic in Cos-7. (**a**) Leukemic (K562) and Breast cancer (1471.1) cells exhibit elevated background ROS as compared to Cos-7. ROS detection assay using the general oxidative stress indicator carboxy-H_2DCFDA conversion to DCF by monitoring on a fluorescent plate reader with excitation at 485 nm and emission at 530 nm. Fluorescence signal was stable across samples and over time when the endpoint reading was collected. One-way ANOVA with Tukey's post-test (error bars are ± S.E.M, $N=3$). (**b**) Representative images of E-cMTS in K562, Cos-7 and 1471.1 cells. The cMTS is selectively targeted to the mitochondria in cells with elevated oxidative stress. ROS activate PKC kinases that, in turn, activate, via phosphorylation, the cMTS. The phosphorylated "active" cMTS translocates from the cytoplasm to the mitochondria. Channel one (EGFP) and channel two (MitoTracker) have been false colored, cyan and magenta, respectively, for increased visual clarity. Colocalized pixels in merged cyan and magenta images show as white. The 'Colormap' (far right column) displays positively correlated pixels in hot colors and negatively correlated pixels in cold colors that can be interpreted using the color scale bar (shown at bottom of the 'Colormap' column). Scale bars are 5 μm. (mean PCC values are ± S.E.M, $N=3$) (**c**) Individual cell ROIs were selected from confocal images taken with live cells and analyzed using the PCC to quantify the degree of E-cMTS mitochondrial colocalization in K562, 1471.1 and Cos-7 cells. Signal from EGFP (tagged to cMTS) and MitoTracker Red CM-H_2XRos staining were compared. One-way ANOVA with Tukey's post-test (error bars are ± S.E.M, $N=3$, $P<0.01$**, $P<0.001$***).

represented by Pearson's correlation coefficient (PCC) (29). EGFP-C1 was used as a negative control for colocalization studies (thresholded PCC values of EGFP-C1 and MitoTracker CMXros in the different cell lines were, K562: −0.20±0.13, Cos-7: 0.04±0.03, and 1471.1: 0.116±0.03). Mitochondrial colocalization of constructs was verified to be consistent at different cell depths (i.e., z-plane sections; data not shown). Although overlay of the E-cMTS and MitoTracker

CMXros signals are provided ('Merge' column) for visual assessment of pixel overlap, a superior visual representation of colocalization, showing spatial depiction of pixel overlap and relative intensity, can be seen in the 'colormap' column (31).

As a control for baseline translocation efficiency across cell types, in a PKC and PKA independent manner, a canonical MTS derived from Bcl-X_L was subcloned into EGFP-C1 (E-MOM), Fig. 2. The Bcl-X_L has been demonstrated to efficiently translocate heteroproteins to the mitochondrial outer membrane (MOM) (34). The MTSs from both the cMTS and Bcl-X_L are C-terminal sequences. The Bcl-X_L MTS targets to the MOM (35) whereas the cMTS is targeted to the mitochondrial matrix (15). Images in Fig. 3a display the robust mitochondrial targeting efficiencies of E-MOM in each of the three cell lines used. Analysis of images evaluating E-MOM mitochondrial localization collected in three separate experiments (Fig. 3b) confirm that the translocation machinery of K562, 1471.1 and Cos-7 cells is sufficiently proficient for comparison of cMTS localization in these cell types.

Requirement for Threonine 193 but not Serine 189 for Mitochondrial Translocation of cMTS in K562 and 1471.1 Cells

Two cMTS mutants were made in order to determine the importance, in K562 and 1471.1 cells, of previously determined PKA (S189) and PKC (T193) phosphorylation sites that lead to the activation and mitochondrial accumulation

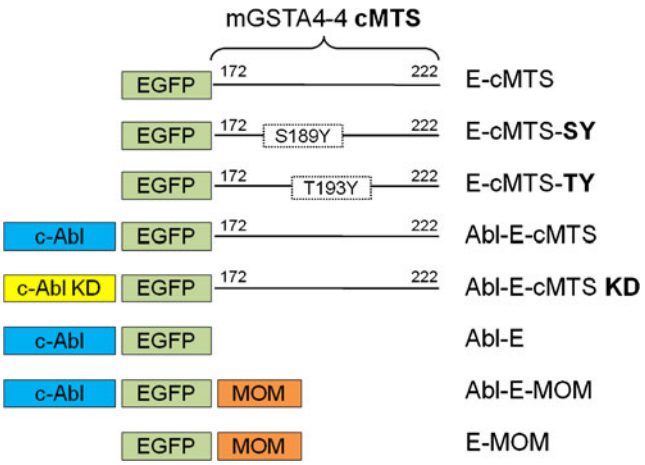

Fig. 2 Diagram of constructs. The C-terminal 50-amino acid sequence of mGSTA4-4 was fused to the C-terminus of EGFP to create, E-cMTS. The PKA and PKC phosphorylation site-mutants are E-cMTS-SY and E-cMTS-TY, respectively. Abl-E serves as a negative control for mitochondrial translocation and a baseline for cell death upon mitochondrial targeting of c-Abl/MTS constructs. Abl-E was constructed with c-Abl positioned N-terminally to the EGFP tag in order to maintain c-Abl's ability to adopt a native auto-inhibitory conformation (14). Abl-E-MOM and E-MOM contain a canonical MTS derived from Bcl-X_L that targets to the mitochondrial outer membrane (MOM). Abl-E-cMTS KD is the cMTS fused to a kinase dead c-Abl.

of the cMTS (Table 1, E-cMTS-SY and E-cMTS-TY, respectively) (15). The mutations to the PKA and PKC phosphorylation sites were changed to minimal c-Abl tyrosine kinase recognition sequences because of the possibility that Bcr-Abl tyrosine kinase activity in K562 cells could modulate the mitochondrial localization of a mutant cMTS via tyrosine phosphorylation. However, Bcr-Abl does not activate the mutant cMTS's (Fig. 4b, 5th column to the right (E-cMTS-TY does not accumulate in the mitochondria of Bcr-Abl positive K562 cells) and Fig. 5c, 7th column (the kinase inhibitor imatinib does not prevent the mitochondrial accumulation of E-cMTS-SY)). Mutating the PKA phosphorylation site S189 to tyrosine and further altering the three residues proceeding the serine at position at 189 (E-cMTS-SY, see Table 1, underlined) did not have an effect on mitochondrial localization in either 1471.1 or K562 cells as compared to E-cMTS (Fig. 4b, compare 1st and 2nd set of columns). However, the T193Y mutation (E-cMTS-TY), interrupting the PKC phosphorylation site, ablated mitochondrial localization in both K562 and 1471.1 cell lines (Fig. 4b, compare 1st and 3rd set of columns). The cMTS mutant data implicates PKC, and not PKA, as a critical activator of the cMTS in K562 leukemia and 1471.1 breast cancer cell lines. Qualitatively, the differences in mitochondrial localization between the E-cMTS-SY (Fig. 4a, top two rows) and E-cMTS-TY (Fig. 4a, bottom two rows) mutants in K562 and 1471.1 cells can be seen. Instead of tyrosine mutations we also tested alanine mutations (as done previously (15)) at positions 189 and 193 and obtained similar results (data not shown).

Imatinib Induces, While α-Tocopherol and N-Acetylcysteine Reduce, Both ROS and Mitochondrial Localization of the E-cMTS in K562 Cells

It is well established that imatinib (IM) treatment induces ROS production (36). Imatinib treatment (10 μM) produced a 160 % rise in ROS after 24 h in K562 cells (versus untreated K562 cells, Fig. 5a, compare 2nd to 1st column). The converse was seen with antioxidant treatment, using either 50 μM α-tocopherol (α-Toc) or 5 mM N-acetylcysteine (NAC) for 24 h, which brought about a decline (~30 %) in measured ROS against control K562 (Fig. 5a, compare 3rd and 4th columns to 1st). A concentration of 300 μM NAC was also used in K562 cells but it did not result in a significant decrease in ROS (Fig. 5a, 5th column). In addition to its antioxidant effects, α-tocopherol also has an independent inhibitory effect on PKC family members (37). Previously, a physiological concentration of α-tocopherol (50 μM) reduced phorbol ester-stimulated cell adhesion in K562 cells to the same degree as a specific PKC inhibitor, Calphostin C (38). Hydrogen peroxide (500 μM,

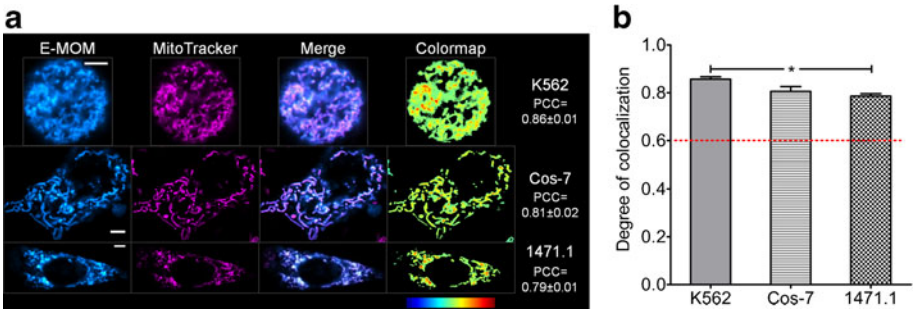

Fig. 3 The translocation efficiency for the cell types tested is sufficient to determine mitochondrial localization of constructs. Using a canonical MTS derived from Bcl-X_L fused to EGFP, the relative capability of each cell type was determined. (**a**) Representative images of K562, Cos-7, and 1471.1 cells transfected with E-MOM construct at 24 h. (**b**) Signal from E-MOM and MitoTracker Red CM-H_2XRos staining were compared. One-way ANOVA with Tukey's post-test (error bars are ± S.E.M., $N=3$, $P<0.05$*).

24 h), as a positive control, generated a 3-fold induction of ROS (data not shown) above that of untreated K562 cells.

Imatinib and antioxidant treatment altered E-cMTS mitochondrial localization corresponding to the assessed ROS levels (compare Fig. 5a, for the ROS level difference between imatinib and antioxidant treated K562 and corresponding degree of mitochondrial localization in Fig. 5c). Correlation analysis between E-cMTS mitochondrial localization and ROS level (Fig. 6) generated an $R^2=0.62$ ($P<0.05$) across each cell type and K562 cells treated with imatinib and antioxidants. The correlation between E-cMTS mitochondrial localization and basal ROS level for the 1471.1 breast cancer cell line falls outside of the 95 % confidence band. This is not unexpected as high PKC activity or expression is associated with rapidly proliferating breast cancer cell lines (39). Higher mitochondrial localization of E-cMTS (PCC: 0.89±0.01) was seen with imatinib while α-tocopherol (PCC: 0.50±0.02) lowered E-cMTS mitochondrial localization as compared to untreated (PCC: 0.78±0.02) in K562 cells (Fig. 5c). Similar to α-tocopherol treatment of K562 cells, the E-cMTS decreased mitochondrial association when treated with either 5 mM NAC (Fig. 5c, 4th column (PCC: 0.49±0.04)) or 300 μM NAC (Fig. 5c, 5th column (PCC: 0.60±0.02)). The imatinib related increase in mitochondrial association was also seen with the E-cMTS-SY mutant (Fig. 5c, compare 6th and 7th columns) but not with the E-cMTS-TY mutant which remained cytoplasmic (PCC: 0.35±0.2 and 0.23±0.2, with and without imatinib, respectively) in K562 cells. There was no difference in the mitochondrial distribution of E-cMTS-TY in imatinib treated and untreated K562 cells. The E-cMTS-SY mutant is exclusively phosphorylated by PKC at the T193 position (15). The contrast in mitochondrial localization between the E-cMTS-SY and E-cMTS-TY mutants, in the presence of imatinib, further clarifies the relative importance of PKC over PKA mediated activation of the cMTS by antineoplastic induced ROS.

As noted above, the mutants incorporating the minimal c-Abl tyrosine kinase consensus sequence (either at around residue position 189 (E-cMTS-SY) or 193 (E-cMTS-TY); Table 1) are not targeted to the mitochondria by the activity of Bcr-Abl (c-Abl). This is confirmed by the increased mitochondrial colocalization of the E-cMTS-SY in the presence of the tyrosine kinase inhibitor, imatinib at a saturating concentration of 10 μM. Representative images of E-cMTS mitochondrial localization in K562 cells upon imatinib (Fig. 5b, top row), α-tocopherol (Fig. 5b, middle row), or N-acetylcysteine (NAC 5 mM: Fig. 5b, bottom row) treatment show the different intracellular distribution profiles.

Table I Names of cMTS Constructs, Corresponding Residue Sequences, Relevant Protein Kinase, and Key Residue Mutation

Construct	cMTS Sequence: mGSTA4-4 C-terminal residues 172-222	Phosphorylation by:	Key residue mutation
cMTS	APVLSDFPLLQAFKTRI**S**NIP**T**IKKFLQPGSQRKPPPDGPYVEVVRTVLKF	PKA/PKC	none
cMTS-SY	APVLSDFPLLQAFKEAI**Y**NIPTIKKFLQPGSQRKPPPDGPYVEVVRTVLKF	PKC only	S189Y
cMTS-TY	APVLSDFPLLQAFKTRISNII**Y**IKKFLQPGSQRKPPPDGPYVEVVRTVLKF	PKA only	T193Y

C-terminal 50-amino acid sequence of mGSTA4-4; PKA (S189) and PKC (T193) phosphorylation sites are bolded. cMTS-SY has a key mutation (S189Y) creating a PKA-null site-mutant whereas cMTS-TY contains a key mutation (T193Y) creating a PKC-null site-mutant. Residues underlined in black were also mutated to incorporate the minimal c-Abl phosphorylation consensus recognition sequence while simultaneously ablating either the PKA or PKC phosphorylation sites. The cMTS-SY and cMTS-TY mutations, computationally analyzed for potential changes to the secondary structure via the MPI Bioinformatics Toolkit (50), did not alter the secondary structure (i.e., α-helicity, disordered regions, or solvent accessibility) as compared to wild-type cMTS. Incorporation of both the S189Y and T193Y mutations into the cMTS resulted in a strictly cytosolic distribution of the cMTS-SY/TY mutant generating a thresholded PCC of 0.14±0.2 in K562 cells when compared to MitoTracker CMXros.

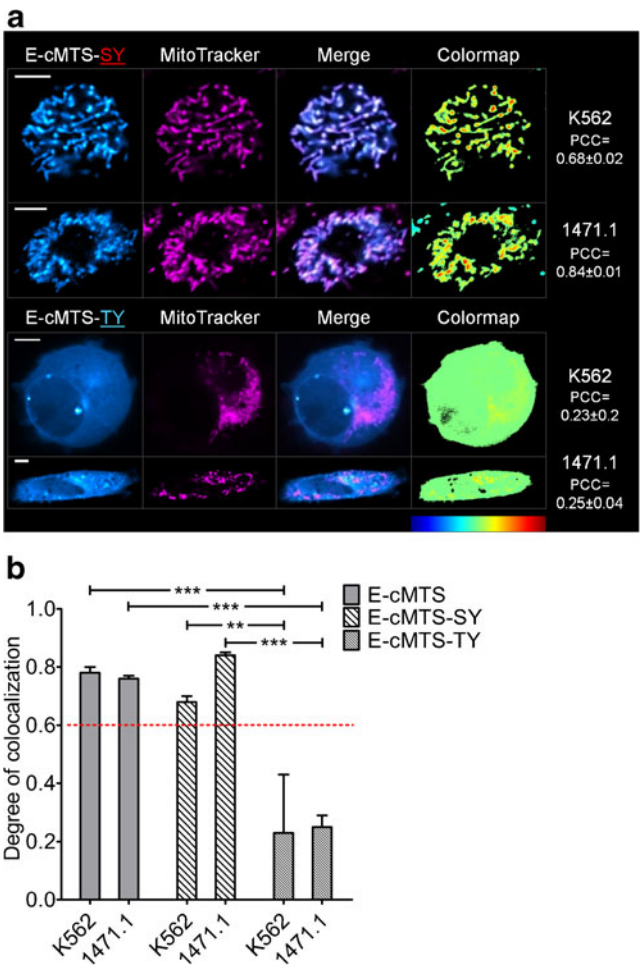

Fig. 4 The conserved threonine 193 is critical for mediating mitochondrial localization under oxidative conditions. (**a**) EGFP-tagged cMTS-SY and cMTS-TY were compared to MitoTracker Red CM-H_2XRos staining in live cells. EGFP and MitoTracker channels were false-colored cyan and magenta, respectively, for increased visual clarity. Colormap displays spatial intensity correlation between channels. Scale bar is 5 μm. (mean PCC values are ± S.E.M, N=3) (**b**) Mitochondrial localization of wild-type E-cMTS as compared to mutated E-cMTS-SY (S189Y) and E-cMTS-TY (T193Y) in K562 and 1471.1 cells. In both 1471.1 and K562 cells the cMTS was not statistically different from E-cMTS-SY. Two-way ANOVA with Bonferroni post-test (error bars are ± S.E.M., N=3, $P<0.01$**, $P<0.001$***).

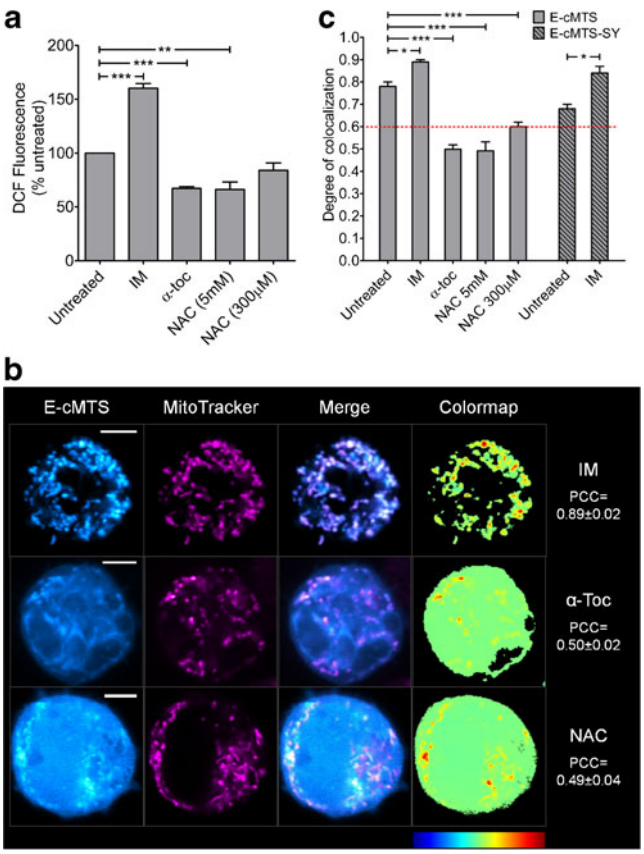

Fig. 5 Imatinib increases, while antioxidants α-tocopherol and N-acetylcysteine attenuate, ROS and E-cMTS mitochondrial colocalization in K562 cells. (**a**) Comparison of ROS levels between K562 cells treated with imatinib (10 μM, IM), α-tocopherol (50 μM, α-toc), or N-acetylcysteine (300 μM or 5 mM, NAC) for 24 h. Values are expressed as a percent of untreated K562 cells. One-way ANOVA with Dunnett's post-test (error bars are ± S.E.M, N=3) (**b**) Representative images of live K562 cells transfected with E-cMTS and treated with imatinib, α-tocopherol, or NAC compared to MitoTracker Red CM-H_2XRos staining. Scale bar is 5 μm. (mean thresholded PCC values are ± S.E.M, N=3) (**c**) Mitochondrial association of the E-cMTS or E-cMTS-SY in K562 cells after 24 h of treatment with imatinib (10 μM) or E-cMTS with α-tocopherol (50 μM) and N-acetylcysteine (NAC; 300 μM and 5 mM). The imatinib induced ROS in K562 cells corresponds to the increased mitochondrial accumulation of both E-cMTS and E-cMTS-SY (mutant with PKC phosphorylation site only). Likewise, α-tocopherol and 5 mM NAC treated cells demonstrated lower overall mitochondrial association which corresponds to lower ROS levels. E-cMTS transfected groups (*A* and *C*): one-way ANOVA with Tukey's post-test and E-cMTS-SY group (*C*): two-tailed unpaired t-test (error bars are ± S.E.M., N=3, $P<0.05$*, $P<0.01$**, $P<0.001$***).

Abl-E-cMTS Selectively Targets the Mitochondria of Cells with Higher Oxidative Backgrounds

The c-Abl protein was fused to the N-terminus of the cMTS (Abl-E-cMTS) (see Fig. 3) and transiently transfected into K562, Cos-7, and 1471.1 cells. The Abl-E construct (no MTS) was used as a negative control (in K562 (Fig. 7a, top row and 7b, first column) and Cos-7 cells (PCC: −0.26±0.06)). The c-Abl fusion to the cMTS colocalized with the mitochondria in K562 and 1471.1 cells similarly to cMTS alone (compare Fig. 1c, 1st and 3rd columns with Fig. 7b, 2nd and 4th columns). This was not expected for the c-Abl-E-cMTS because c-Abl has many cytosolic and nuclear binding partners (40). Also, as with the cMTS alone the Abl-E-cMTS remained cytosolic in Cos-7 cells (Fig. 1c, 2nd row (PCC=0.18±0.06) and Fig. 7b, 3rd row (PCC= 0.13±0.08), respectively).

The same C-terminal canonical MTS derived from Bcl-X_L, as used above, was also fused to c-Abl-E (Fig. 2) as a control for mitochondrial translocation efficiency of c-Abl across cell types and assessment of functional consequences accompanying ROS selective mitochondrial targeting via the cMTS. Although there was a significant difference in

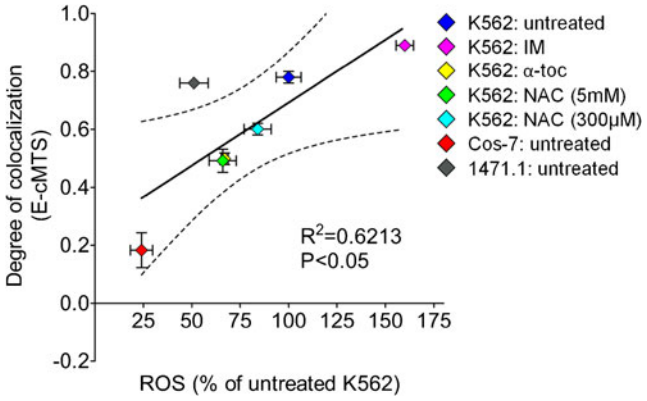

Fig. 6 Correlation analysis between ROS level and the 'degree of colocalization'. Correlation analysis demonstrated a connection between ROS level and mitochondrial localization of the E-cMTS. Since PKC mediates the ROS activation of the E-cMTS an altered ROS-to- mitochondrial localization relationship for E-cMTS is to be expected to be contingent upon the varying level of PKC expression and activity of PKC within a given cell type. The R^2 value when considering only the K562 cell line was 0.877 ($P < 0.05$).

mitochondrial colocalization coefficients between K562 and Cos-7 (Fig. 7d, compare 1st and 2nd columns; $P < 0.05$), the PCC values for all three cell lines exceeded the 0.6 colocalization threshold for Abl-E-MOM. Importantly, there was no difference between E-MOM and Abl-E-MOM colocalization for any of the cell lines as expected. Representative images of K562, Cos-7, and 1471.1 cells transfected with Abl-E-MOM and stained with MitoTracker CMXros showing mitochondrial localization can be seen in Fig. 7c.

Targeting c-Abl to the Mitochondrial Matrix is Toxic to K562 Leukemia but not 1471.1 Breast Cancer Cell Lines

To assess the functional significance at the level of cell death induction from mitochondrial c-Abl, cell lines were transiently transfected with the c-Abl containing constructs or controls (Fig. 2), stained with 7-AAD, and fluorescence measured via flow cytometry at 48 h after transfection. The effects of the constructs were analyzed for each cell type (Fig. 8, a-c). First, there was no difference between any of the constructs and measured cell death in Cos-7 cells (Fig. 8b). Secondly, 1471.1 cells (Fig. 8c) did not exhibit any significant difference in cell death between cytoplasmic c-Abl (i.e., Abl-E) and mitochondrially localized c-Abl (i.e., Abl-E-MOM and Abl-E-cMTS). Finally, K562 cells (Fig. 8a) are killed by mitochondrial c-Abl but only if targeted to the matrix (Abl-E-cMTS). Targeting c-Abl to the outer membrane induces death to the same level as either cytoplasmic c-Abl (Abl-E) or the cMTS alone (E-cMTS). A kinase dead mutant (25) of c-Abl (Abl-E-cMTS KD) trended lower but did not reach significance from Abl-E-cMTS nor

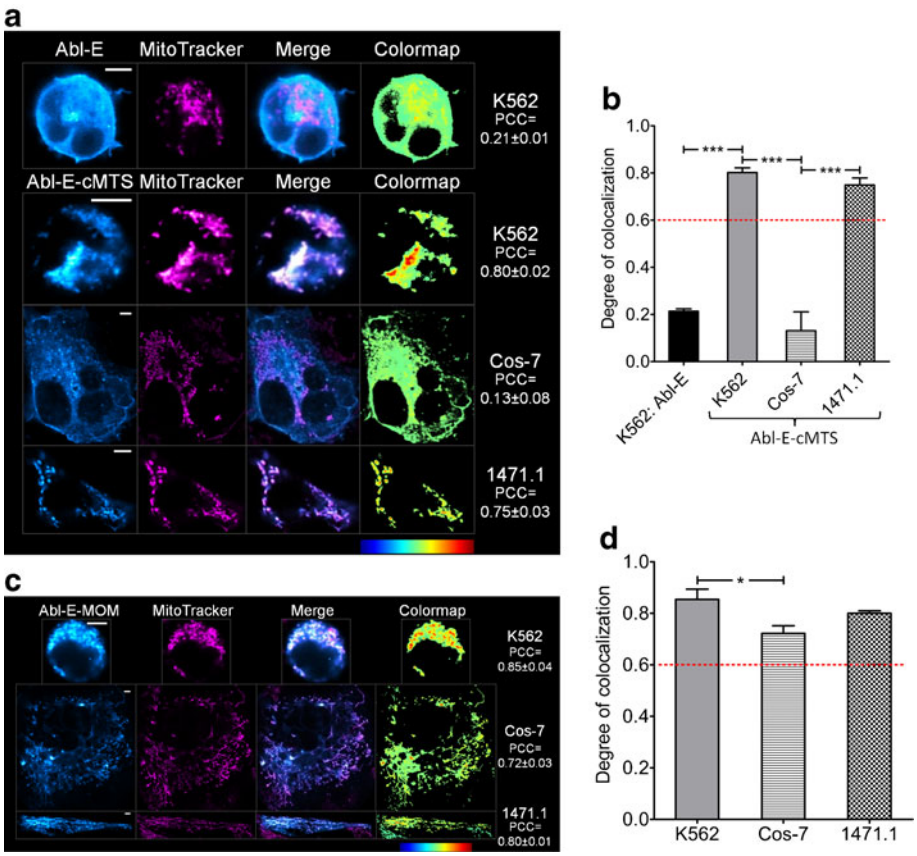

Fig. 7 The cMTS selectively targets c-Abl to the mitochondria of cells that have elevated oxidative backgrounds. (**a**) Abl-E-cMTS and Abl-E were compared to MitoTracker Red CM-H_2XRos staining in live cells. EGFP and MitoTracker channels were false-colored cyan and magenta, respectively, for increased visual clarity. Scale bar is 5 μm. (mean thresholded PCC values are ± S.E.M, $N=3$) (**b**) Abl-E-cMTS localized to the mitochondria of 1471.1 and K562 but not Cos-7 cells. Without the cMTS, Abl-E does not localize to the mitochondria of K562 cells. (**c**, **d**) Unlike the cMTS, the MOM robustly directs c-Abl to the mitochondria of each cell type. *C*) Representative images of K562, Cos-7, and 1471.1 cells transfected with Abl-E-MOM construct at 24 h. One-way ANOVA with Tukey's post-test (error bars are ± S.E.M., $N=3$, $P < 0.05$*, $P < 0.001$***).

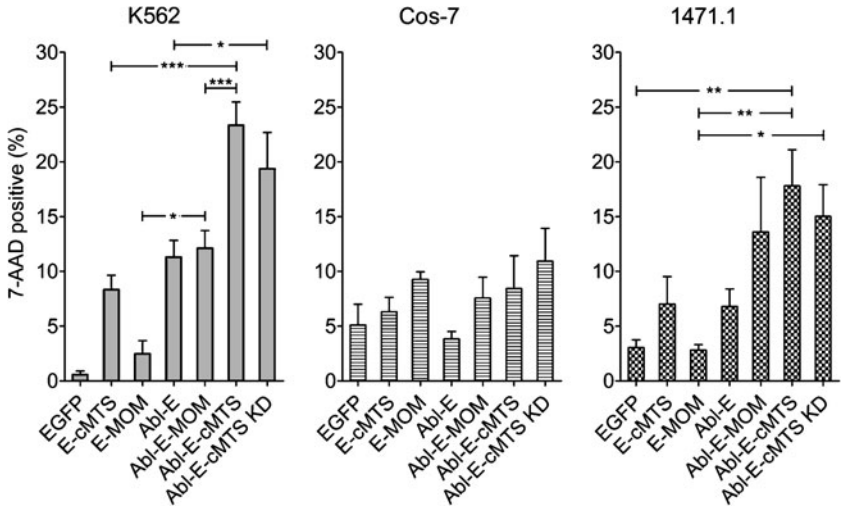

Fig. 8 c-Abl is selectively induces cell death in K562 leukemia cells when targeted to the mitochondrial matrix. (**a**) K562 leukemia cells: K562 leukemia cells were highly susceptible to cell death caused by c-Abl in the mitochondrial matrix (Abl-E-cMTS) but not at the mitochondrial outer membrane (Abl-E-MOM). (**b**) Cos-7 fibroblast cells: In Cos-7 cells, neither cytoplasmic nor mitochondrially targeted c-Abl induced cell death. (**c**) 1471.1 breast cancer cells: There was an increase ($P < 0.01$) in cell death for Abl-E-cMTS over the 'non-toxic' EGFP and E-MOM controls in 1471.1 cells. However, there was no difference between the mitochondrially localized c-Abl and cMTS. (B-D: One-way ANOVA with Tukey's post-test; A-D: error bars are ± S.E.M., $N \geq 3$, $P < 0.05$*, $P < 0.01$**, $P < 0.001$***).

was it different from cytoplasmic Abl-E. Taken together the data suggest a cell type dependent susceptibility to the cell death effects of c-Abl targeted to the mitochondrial matrix. Although there is no statistical difference between the EGFP control and the E-cMTS (Fig. 8a, compare 1st and 2nd columns) in K562 cells, this "trend" in mild toxicity associated with the mitochondrial targeting of EGFP regardless of MTS is a common occurrence that we have noticed in several of our studies across multiple cell types (41). This trend, when viewed between K562 and 1471.1 cells (Fig. 8a, c) may be indicative of a phenomenon termed 'mitochondrial priming' whereby the mitochondria set the cell death threshold via a balance between pro-survival and pro-apoptotic Bcl-2 family members, in a rheostat like manner (42). Cell death exhibited across constructs in 1471.1 cells was lower than expected (as compared to K562). However, overall profiles for cell death between K562 and 1471.1 look very similar but the scale of cell death is reduced in 1471.1 cells. It is possible that the mitochondria of K562 cells are more susceptible to a mitochondrial insult such as c-Abl. Future studies investigating the level of 'primed' mitochondrial status between K562 and 1471.1 would be very useful for optimizing therapeutic agents targeted to the mitochondria.

This study represents (to our knowledge) the first time c-Abl has been directly targeted to the mitochondria (instead of by a pharmacological or UV/IR insult). Furthermore, we show that c-Abl may exert its pro-apoptotic effect at the mitochondrial matrix. Our laboratory has developed an intracellular chaperone designed to bind and target the oncoprotein Bcr-Abl to the mitochondria. This study served as a proof of concept for using the central etiologic agent of chronic myelogenous leukemia (Bcr-Abl) to, in essence, self-destruct the diseased cells via the mitochondrial apoptotic pathway.

DISCUSSION

Our laboratory has previously developed a protein switch capable of translocating a protein from the cytoplasm to the nucleus upon ligand induction (43). Here we show that the cMTS acts as a mitochondrial protein switch, translocating from the cytoplasm to the mitochondria as a condition of elevated ROS inherent in K562 leukemic and 1471.1 breast cancer line phenotypes. The C-terminal cMTS is particularly useful for targeting the sensitive proto-oncoprotein c-Abl to the mitochondria of K562 cells because any fusion to the N-terminus will disrupt the ability of c-Abl to adopt its native conformation (44). The fusion of the BCR gene to the ABL gene creates Bcr-Abl, the etiological cause of chronic myelogenous leukemia, disrupting c-Abl's autoinhibitory conformation generating a constitutively active Abl tyrosine kinase (44). The kinase activity of c-Abl is necessary and sufficient for the induction of apoptosis, and c-Abl has a critical role at the mitochondria in apoptotic induction (45,46). Previous studies of c-Abl translocating to the mitochondria have been indirect, through the induction of apoptosis/cell stress (e.g., hydrogen peroxide, etoposide, tunicamycin (45)). This study investigated the *in vitro* cell death consequences of direct mitochondrial targeting of c-Abl using MTSs in the context of varying levels of basal oxidative stress.

Likewise, protein kinase stimulators (e.g., cAMP and phorbol ester) were used previously for activating the mitochondrial targeting of the cMTS fused to a heteroprotein (dihydrofolate reductase) in Cos cells (15). However, we demonstrate that the cMTS can robustly target the mitochondria of K562 and 1471.1 cancer cell lines without pharmacological induction. Therefore, the cMTS may confer specific targeting of heteroproteins (c-Abl) to the mitochondria in cells exhibiting elevated ROS/PKC activity. Further work will need to be done to identify which PKC isoforms are contributing the phosphorylation of the cMTS and if these are the same isoforms that often overexpressed in cancer (e.g., breast). Yet, the mitochondrial targeting of the cMTS can be attenuated or enhanced by antioxidant or antineoplastic treatment, respectively. We are interested in elucidating the functional consequences of targeting c-Abl to the mitochondria in a leukemia specific context, and the cMTS provides an effective way to accomplish this in a selective manner. To this end, we were intrigued to find the difference in cell death induction efficacy between c-Abl targeted to the mitochondrial matrix versus the outer membrane of the leukemia cell line. A similar cell death phenomenon occurred when p53 was directly targeted to the mitochondrial matrix and outer membrane using MTSs (47). There may be a correspondence between susceptibility to cell death when c-Abl is localized to the mitochondrial matrix and ROS level (1). However, this will require further investigation.

We used the cMTS as a vehicle to selectively deliver c-Abl under conditions of oxidative stress in a cancer context, but the implications of the cMTS utility could be expanded upon. For instance, c-Abl's role at the mitochondria is currently being investigated in other conditions with pathological ROS such as neurodegenerative disease (48) and diabetes (49). Additionally, the cMTS may be of benefit to selectively target either pro-apoptotic or pro-survival factors (e.g., BH3 mimetics or antioxidant enzymes) to the mitochondria to elicit or prevent cell death, respectively.

Considering future directions, if the Abl-cMTS were delivered *in vivo*, perhaps via adenoviral vector delivery, it would confer a level of selectivity for mitochondrial accumulation in cells with elevated oxidative stress. Additionally, our results indicate that the Abl-cMTS is toxic to leukemic cells and much less so in non-leukemic cell lines.

ACKNOWLEDGMENTS & DISCLOSURES

We acknowledge the use of the University of Utah, School of Medicine, Cell Imaging Facility and would like to thank the Director, Chris Rodesch, PhD, for scientific discussions. We would also like to thank Karina Matissek, Geoffrey Miller, and Dr. Andy Dixon for scientific discussions. The Core Facilities described in this project were supported by Award Number P30CA042014 from the National Cancer Institute. The content is solely the responsibility of the authors and does not necessarily represent the official views of the National Cancer Institute or the National Institutes of Health. The authors declare that they have no competing interests. This work was funded by NIH R01-CA129528 and by an AFPE Pre-Doctoral Fellowship (JEC).

REFERENCES

1. Ralph SJ, Rodriguez-Enriquez S, Neuzil J, Saavedra E, Moreno-Sanchez R. The causes of cancer revisited: "mitochondrial malignancy" and ROS-induced oncogenic transformation - why mitochondria are targets for cancer therapy. Mol Aspects Med. 2010;31(2):145–70.
2. Szabadkai G, Rizzuto R. Chaperones as parts of organelle networks. Adv Exp Med Biol. 2007;594:64–77.
3. Certo M, Del Gaizo Moore V, Nishino M, Wei G, Korsmeyer S, Armstrong SA, *et al.* Mitochondria primed by death signals determine cellular addiction to antiapoptotic BCL-2 family members. Cancer Cell. 2006;9(5):351–65.
4. Wang JY. Nucleo-cytoplasmic communication in apoptotic response to genotoxic and inflammatory stress. Cell Res. 2005;15 (1):43–8.
5. Ito Y, Pandey P, Mishra N, Kumar S, Narula N, Kharbanda S, *et al.* Targeting of the c-Abl tyrosine kinase to mitochondria in endoplasmic reticulum stress-induced apoptosis. Mol Cell Biol. 2001;21(18):6233–42.
6. Gupta M, Milani L, Hermansson M, Simonsson B, Markevarn B, Syvanen AC, *et al.* Expression of BCR-ABL1 oncogene relative to ABL1 gene changes overtime in chronic myeloid leukemia. Biochem Biophys Res Commun. 2008;366(3):848–51.
7. Sirvent A, Benistant C, Roche S. Cytoplasmic signalling by the c-Abl tyrosine kinase in normal and cancer cells. Biol Cell. 2008;100 (11):617–31.
8. Kumar S, Bharti A, Mishra NC, Raina D, Kharbanda S, Saxena S, *et al.* Targeting of the c-Abl tyrosine kinase to mitochondria in the necrotic cell death response to oxidative stress. J Biol Chem. 2001;276(20):17281–5.
9. Qi X, Mochly-Rosen D. The PKCdelta -Abl complex communicates ER stress to the mitochondria - an essential step in subsequent apoptosis. J Cell Sci. 2008;121(Pt 6):804–13.
10. Salvi M, Brunati AM, Toninello A. Tyrosine phosphorylation in mitochondria: a new frontier in mitochondrial signaling. Free Radic Biol Med. 2005;38(10):1267–77.
11. Kumar S, Mishra N, Raina D, Saxena S, Kufe D. Abrogation of the cell death response to oxidative stress by the c-Abl tyrosine kinase inhibitor STI571. Mol Pharmacol. 2003;63 (2):276–82.
12. Horbinski C, Chu CT. Kinase signaling cascades in the mitochondrion: a matter of life or death. Free Radic Biol Med. 2005;38 (1):2–11.
13. Sangar MC, Bansal S, Avadhani NG. Bimodal targeting of microsomal cytochrome P450s to mitochondria: implications in drug metabolism and toxicity. Expert Opin Drug Metab Toxicol. 2010;6(10):1231–51.
14. Quintas-Cardama A, Cortes J. Molecular biology of bcr-abl1-positive chronic myeloid leukemia. Blood. 2009;113(8):1619–30.

15. Robin MA, Prabu SK, Raza H, Anandatheerthavarada HK, Avadhani NG. Phosphorylation enhances mitochondrial targeting of GSTA4–4 through increased affinity for binding to cytoplasmic Hsp70. J Biol Chem. 2003;278(21):18960–70.
16. Raza H, Robin MA, Fang JK, Avadhani NG. Multiple isoforms of mitochondrial glutathione S-transferases and their differential induction under oxidative stress. Biochem J. 2002;366(Pt1):45–55.
17. Gupta SC, Hevia D, Patchva S, Park B, Koh W, Aggarwal BB. Upsides and Downsides of Reactive Oxygen Species for Cancer: The Roles of Reactive Oxygen Species in Tumorigenesis, Prevention, and Therapy. Antioxid Redox Signal. 2012 [Epub ahead of print].
18. Bair JS, Palchaudhuri R, Hergenrother PJ. Chemistry and biology of deoxynyboquinone, a potent inducer of cancer cell death. J Am Chem Soc. 2010;132(15):5469–78.
19. Kim JH, Chu SC, Gramlich JL, Pride YB, Babendreier E, Chauhan D, *et al.* Activation of the PI3K/mTOR pathway by BCR-ABL contributes to increased production of reactive oxygen species. Blood. 2005;105(4):1717–23.
20. Sattler M, Verma S, Shrikhande G, Byrne CH, Pride YB, Winkler T, *et al.* The BCR/ABL tyrosine kinase induces production of reactive oxygen species in hematopoietic cells. J Biol Chem. 2000;275(32):24273–8.
21. Chang SP, Shen SC, Lee WR, Yang LL, Chen YC. Imatinib mesylate induction of ROS- dependent apoptosis in melanoma B16F0 cells. J Dermatol Sci. 2011;62(3):183–91.
22. Brown NS, Bicknell R. Hypoxia and oxidative stress in breast cancer. Oxidative stress: its effects on the growth, metastatic potential and response to therapy of breast cancer. Breast Cancer Res. 2001;3(5):323–7.
23. Morse-Gaudio M, Connolly JM, Rose DP. Protein kinase C and its isoforms in human breast cancer cells: relationship to the invasive phenotype. Int J Oncol. 1998;12(6):1349–54.
24. Dixon AS, Kakar M, Schneider KM, Constance JE, Paullin BC, Lim CS. Controlling subcellular localization to alter function: Sending oncogenic Bcr-Abl to the nucleus causes apoptosis. J Control Release. 2009;140(3):245–9.
25. Ko HS, Lee Y, Shin JH, Karuppagounder SS, Gadad BS, Koleske AJ, *et al.* Phosphorylation by the c-Abl protein tyrosine kinase inhibits parkin's ubiquitination and protective function. ProcNatl Acad Sci USA. 2010;107(38):16691–6.
26. Dixon AS, Constance JE, Tanaka T, Rabbitts TH, Lim CS. Changing the Subcellular Location of the Oncoprotein Bcr-Abl Using Rationally Designed Capture Motifs. Pharm Res. 2012;29 (4):1098–109.
27. Rasband WS. BG subtraction from ROI plugin.;2004. Available from: www.uhnres.utoronto.ca/facilities/wcif/imagej/image_intensity_proce.htm#intensity_BG.
28. Bolte S, Cordelieres FP. A guided tour into subcellular colocalization analysis in light microscopy. J Microsc. 2006;224(Pt 3):213–32.
29. Costes SV, Daelemans D, Cho EH, Dobbin Z, Pavlakis G, Lockett S. Automatic and quantitative measurement of protein-protein colocalization in live cells. Biophys J. 2004;86(6):3993–4003.
30. Barlow AL, Macleod A, Noppen S, Sanderson J, Guerin CJ. Colocalization analysis in fluorescence micrographs: verification of a more accurate calculation of pearson's correlation coefficient. Microsc Microanal. 2010;16(6):710–24.
31. Jaskolski F, Mulle C, Manzoni OJ. An automated method to quantify and visualize colocalized fluorescent signals. J Neurosci Methods. 2005;146(1):42–9.
32. Dixon AS, Miller GD, Bruno BJ, Constance JE, Woessner DW, Fidler TP, *et al.* Improved coiled-coil design enhances interaction with bcr-abl and induces apoptosis. Mol Pharm. 2012;9(1):187–95.
33. Mediavilla MG, Di Venanzio GA, Guibert EE, Tiribelli C. Heterologous ferredoxin reductase and flavodoxin protect Cos-7 cells from oxidative stress. PLoS One. 2010;5(10):e13501.
34. Owens TW, Valentijn AJ, Upton JP, Keeble J, Zhang L, Lindsay J, *et al.* Apoptosis commitment and activation of mitochondrial Bax during anoikis is regulated by p38MAPK. Cell Death Differ. 2009;16(11):1551–62.
35. Kaufmann T, Schlipf S, Sanz J, Neubert K, Stein R, Borner C. Characterization of the signal that directs Bcl-x(L), but not Bcl-2, to the mitochondrial outer membrane. J Cell Biol. 2003;160(1):53–64.
36. Chang SP, Shen SC, Lee WR, Yang LL, Chen YC. Imatinib mesylate induction of ROS- dependent apoptosis in melanoma B16F0 cells. J Dermatol Sci. 2011;62(3):183–91.
37. Ricciarelli R, Tasinato A, Clement S, Ozer NK, Boscoboinik D, Azzi A. alpha-Tocopherol specifically inactivates cellular protein kinase C alpha by changing its phosphorylation state. Biochem J. 1998;334(Pt 1):243–9.
38. Breyer I, Azzi A. Differential inhibition by alpha- and beta-tocopherol of human erythroleukemia cell adhesion: role of integrins. Free Radic Biol Med. 2001;30(12):1381–9.
39. Lonne GK, Cornmark L, Zahirovic IO, Landberg G, Jirstrom K, Larsson C. PKCalpha expression is a marker for breast cancer aggressiveness. Molecular cancer. 2010;9:76.
40. Mitra A, Radha V. F-actin-binding domain of c-Abl regulates localized phosphorylation of C3G: role of C3G in c-Abl-mediated cell death. Oncogene. 2010;29(32):4528–42.
41. Mossalam M, Matissek KJ, Okal A, Constance JE, Lim CS. Direct Induction of Apoptosis
Using an Optimal Mitochondrially Targeted P53. Mol Pharm. 2012 [Epub ahead of print]
42. Reed JC. Cancer. Priming cancer cells for death. Science. 2011;334(6059):1075–6.
43. Kakar M, Davis JR, Kern SE, Lim CS. Optimizing the protein switch: altering nuclear import and export signals, and ligand binding domain. J Control Release. 2007;120(3):220–32.
44. Hantschel O, Superti-Furga G. Regulation of the c-Abl and Bcr-Abl tyrosine kinases. Nat Rev Mol Cell Biol. 2004;5(1):33–44.
45. Qi X, Mochly-Rosen D. The PKCdelta -Abl complex communicates ER stress to the mitochondria - an essential step in subsequent apoptosis. J Cell Sci. 2008;121(Pt6):804–13.
46. Ito Y, Pandey P, Mishra N, Kumar S, Narula N, Kharbanda S, *et al.* Targeting of the c-Abl tyrosine kinase to mitochondria in endoplasmic reticulum stress-induced apoptosis. Mol Cell Biol. 2001;21(18):6233–42.
47. Palacios G, Crawford HC, Vaseva A, Moll UM. Mitochondrially targeted wild-type p53 induces apoptosis in a solid human tumor xenograft model. Cell Cycle. 2008;7(16):2584–90.
48. Schlatterer SD, Acker CM, Davies P. c-Abl in Neurodegenerative Disease. J Mol Neurosci. 2011;45(3):445–52.
49. Hagerkvist R, Sandler S, Mokhtari D, Welsh N. Amelioration of diabetes by imatinib mesylate (Gleevec): role of beta-cell NF-kappaB activation and anti-apoptotic preconditioning. Faseb J. 2007;21(2):618–28.
50. Biegert A, Mayer C, Remmert M, Soding J, Lupas AN. The MPI Bioinformatics Toolkit for protein sequence analysis. Nucleic Acids Res. 2006;34W:335–9.